Supporting information for: Ultrafast Transient Terahertz Conductivity of Monolayer MoS$_2$ and WSe$_2$ Grown by Chemical Vapor Deposition

Callum J. Docherty,[†] Patrick Parkinson,[†] Hannah J. Joyce,[†] Ming-Hui Chiu,[‡] Chang-Hsiao Chen,[¶] Ming-Yang Lee,[¶] Lain-Jong Li,[‡] Laura M. Herz,[†] and Michael B. Johnston[*,†]

Department of Physics, University of Oxford, Clarendon Laboratory, Parks Road, Oxford OX1 3PU, U.K., Physical Science and Engineering Division, King Abdullah University of Science and Technology, Thuwal 23955-6900, Kingdom of Saudi Arabia, and Institute of Atomic and Molecular Sciences, Academia Sinica, Taipei, Taiwan

E-mail: m.johnston@physics.ox.ac.uk

Sheet Charge Density Estimation

The sheet charge density of the MoS$_2$ and WSe$_2$ monolayers used in this study were estimated by fabricating electric double-layer transistors (EDLTs) following the method of Pu *et al.*[1] The areal capacitance C was measured as a function of applied reference voltage V_R and converted to sheet

---

[*]To whom correspondence should be addressed
[†]Department of Physics, University of Oxford, Clarendon Laboratory, Parks Road, Oxford OX1 3PU, U.K.
[‡]Physical Science and Engineering Division, King Abdullah University of Science and Technology, Thuwal 23955-6900, Kingdom of Saudi Arabia
[¶]Institute of Atomic and Molecular Sciences, Academia Sinica, Taipei, Taiwan

charge carrier density using the expression

$$n_{2D} = \frac{C(V_R - V_{th})}{e},$$

where V_{th} is the threshold voltage.[1,2] Note that the reference voltage is the voltage applied between the electrolyte and the monolayer surface and is typically smaller than the gate voltage (see Ref 2 for more information).

The measured areal capacitance and sheet charge carrier density for monolayers of MoS_2 and WSe_2 are shown in Supplementary Figure S1 and Supplementary Figure S2 repectively. The vertical lines indicate the value of V_{th}. Our MoS_2 monolayers were found to be n-type with a areal charge density of $2-3 \times 10^{13}$ cm^{-2}, while our WSe_2 monolayers were found to be ambipolar with hole densities in the range $3-5 \times 10^{13}$ cm^{-2} and electron densities in the range $2-4 \times 10^{13}$ cm^{-2}.
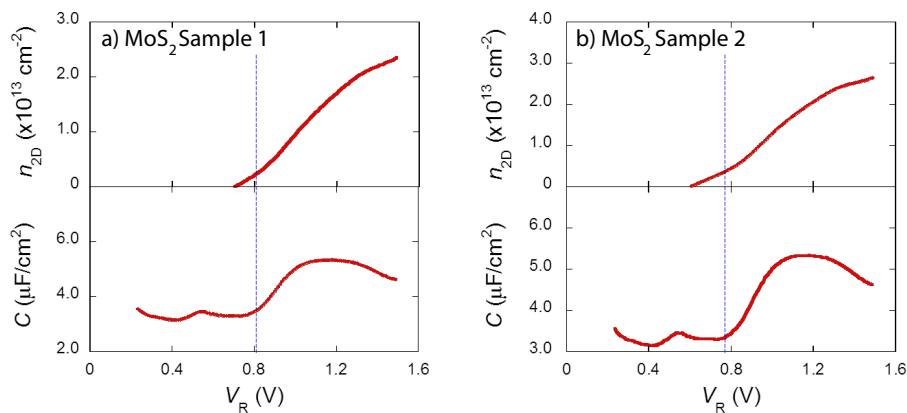

Figure S1: Sheet charge carrier density n_{2D} and areal capacitance C as a function of reference voltage V_R for monolayers of MoS_2 fabricated into electric double-layer transistors. a) and b) show measurements from two different samples. The vertical lines mark the estimated values of the threshold voltages V_{th}.

Optical Pump Terahertz Probe Spectroscopy

The experimental arrangement used for terahertz time domain spectroscopy is displayed in Supplementary Figure S3. The output of a Ti:Sapphire laser amplifier is split into three beams: a pump
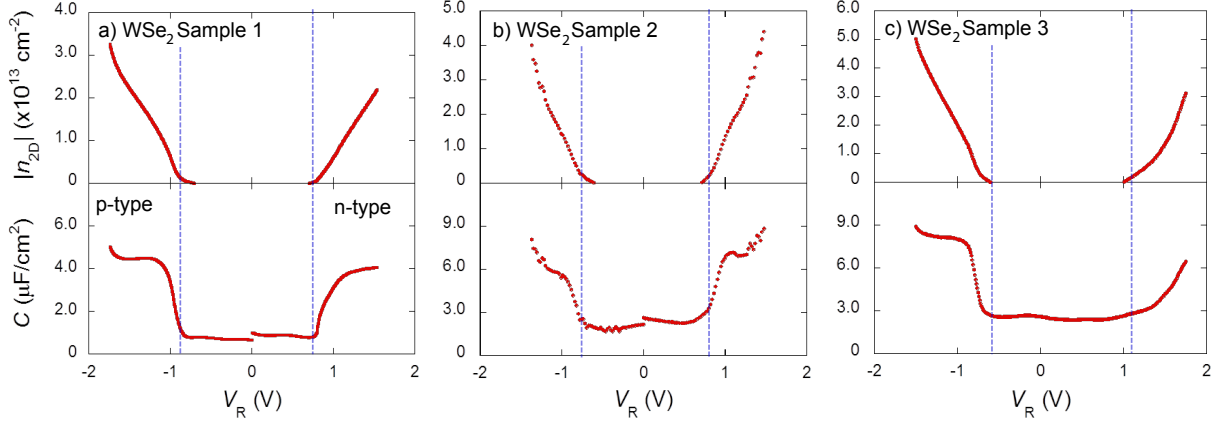
Figure S2: Sheet charge carrier density $|n_{2D}|$ and areal capacitance C as a function of reference voltage V_R for monolayers of WSe$_2$ fabricated into electric double-layer transistors. a) b) and c) show measurements from three different samples. The vertical lines mark the estimated values of the threshold voltages V_{th}.

beam to photoexcite the sample; a terahertz generation beam to produce terahertz radiation by optical rectification in a 2mm GaP crystal; and a gate beam to detect the electric field of the terahertz pulse by electro-optic sampling. Using a quarter waveplate (QP) and a Wollaston prism (WP), the gate beam is separated into two spatially resolved polarisation components for detection by photodiodes (PD), from which the pump induced change in the terahertz signal can be extracted by two lock-in amplifiers, LI1 and LI2, referenced to optical choppers 1 and 2 respectively. The correct phase of the lock-in amplifiers for each experiment is determined by observing the signal from a reference sample with a well known photoresponse (semi-insulating GaAs).

Variable delay stages in the terahertz generation and pump beams allow additional path length to be added to these beams, whereas the gate beam is held fixed. Adding additional path length to the terahertz generation beam alters the time between the arrival of the terahertz pulse and the 35 fs gate pulse at the electro-optic (E-O) crystal, t_1. By varying this time, the full dynamics of the terahertz pulse can be mapped. Alternatively, the time between the pump pulse and the gate pulse, t_2, can be varied. In order to measure the spectrum of the pump-induced transmission change, as in Figure 5 of the main paper, the pump delay time t_2 is set to a fixed value before the terahertz pulse is measured by varying t_1. Thus the delay between the pump pulse and the sampled part of the terahertz pulse is constant. Such data can then be Fourier transformed to yield spectral

information.[3,4] For pump–probe measurements, as in Figure 2 of the main paper, t_1 is held fixed so that only the peak of the terahertz field is detected, whilst varying t_2 to reveal an average of the terahertz response after photoexcitation.
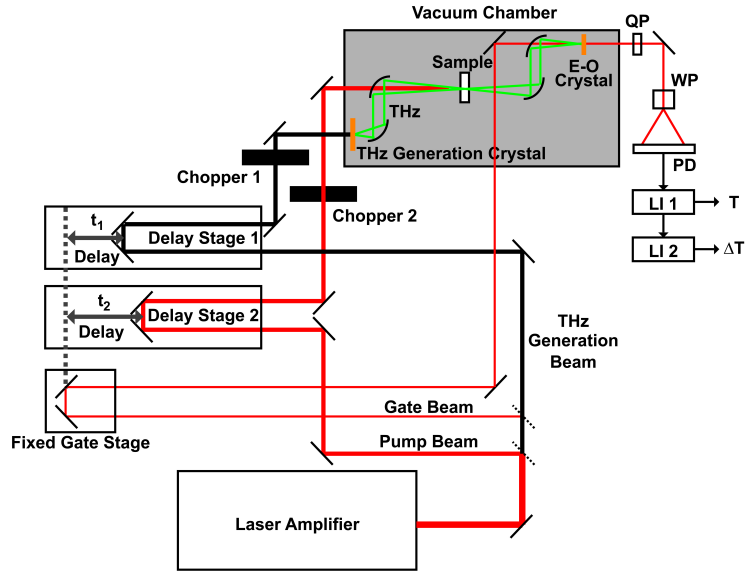

Figure S3: Schematic diagram of the terahertz spectroscopy system used in this study.

THz Transmission Spectra

Although the focus of the main paper is on the *change* in THz transmission due to photoexcitation, it is also possible to measure THz transmission through the non-photoexcited sample. In Supplementary Figure S4a, we present the THz electric field as a function of time passing through the trilayer MoS_2 on sapphire substrate, and the electric field passing through a reference sapphire substrate. These data can be converted to the frequency domain by using a Fourier transform, and the THz amplitude transmission through the MoS_2 film found from $T(\omega) = E_S(\omega)/E_{Ref}(\omega)$, where E_S and E_{Ref} are the Fourier transformed THz electric fields through the sample and the reference respectively.[3,4]

This transmission spectrum is presented in Supplementary Figure S4c. We also present the transmission spectrum obtained when both the sample and reference are missing - i.e. an indication

Table S1: Biexponential decay time constants and relative weightings for pump-probe and PL measurements.

| | THz Photoconductivity | | | PL |
	MoS$_2$ Tri	MoS$_2$ Mono	WSe$_2$ Mono	MoS$_2$ Mono
Above gap	1 ps [90%]	0.33 ps [91%]	1.31 [80%]	0.36 ps [96%]
	24 ps [10%]	33 ps [9%]	13.1 ps [20%]	8.6 ps [4%]
Resonant	0.63 ps [88%]	0.36 ps [95%]	0.861 ps [90%]	0.32 ps [100%]
	10 ps [12%]	35 ps [5%]	15 ps [10%]	–

of the sensitivity of the THz spectrometer. The THz transmission through MoS$_2$ is greater than one at a range of frequencies. This could be due to differences in the thickness of the sample and the reference sapphire, or an antireflection effect due to the thin MoS$_2$ film.

It should be noted, however, that the results in the main paper are from photoconductivity data, where the THz transmission through the MoS$_2$ sample is measured after photoexcitation, and referenced to the THz transmission thorough the same MoS$_2$ sample without photoexcitation. The sensitivity of these photoexcited measurements, detected using a double lock-in method, is therefore much greater than the sensitivity of the transmission presented in Supplementary Figure S4b.

Fitting of Pump–Probe Data

In Figures 2-4 of the main manuscript we presented the photodynamics of mono- and trilayer MoS$_2$, and monolayer WSe$_2$, along with biexponential fits to the photoconductivity and photoluminescence decay. In Supplementary Table 1, we present the details of the fit to the data, detailing the two time constants in each decay along with their relative spectral weightings.

Fitting of THz Photoconductivity Spectra

In Figure 5 of the main paper, we presented THz photoconductivity spectra of the samples taken at 1.5 ps after photoexcitation. The spectrum of the trilayer MoS$_2$ sample appears to have a resonance beyond the experimental bandwidth (4 THz), whilst the spectra of both monolayer MoS$_2$ and WSe$_2$
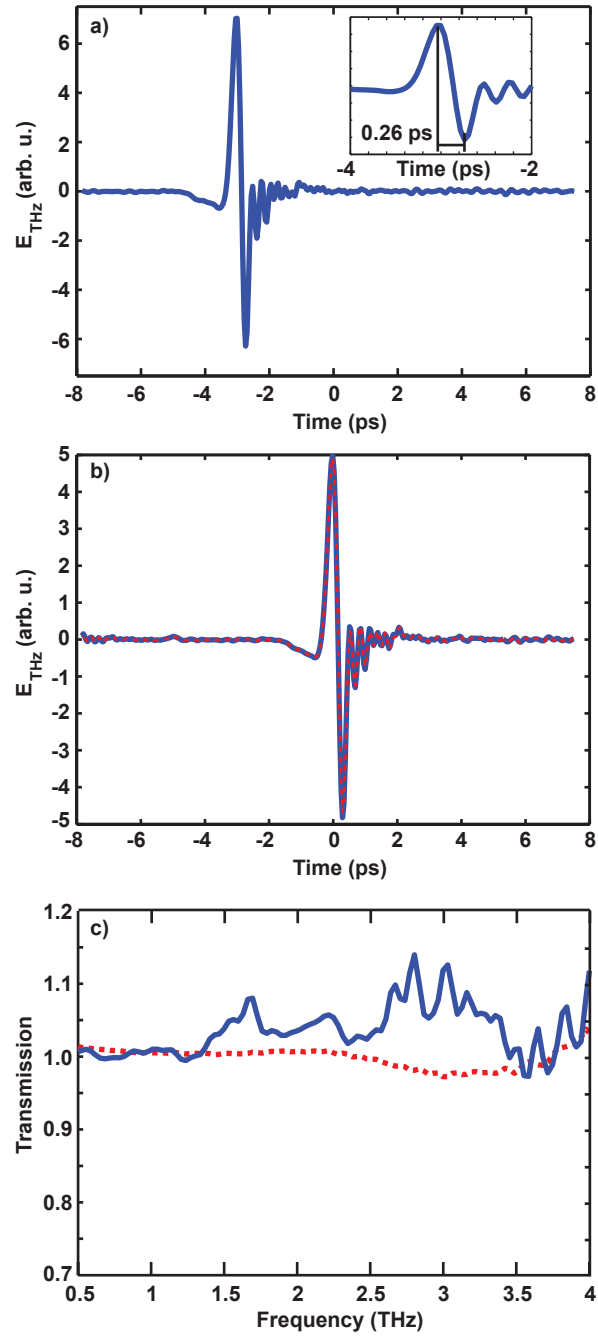
Figure S4: **a)** THz electric field as a function of time passing through vacuum. Inset: Expanded time-axis showing peak to trough duration of 260 fs. **b)** THz electric field as a function of time passing through the trilayer MoS_2 sample on a sapphire substrate (solid blue line) and passing though a reference sapphire substrate (broken red line). **c)** THz amplitude transmission spectrum of trilayer MoS_2 film (solid blue line), and system sensitivity (broken red line).

show resonances (peak in $\text{Re}(\sigma)$ and zero-crossing of $\text{Im}(\sigma)$) at $\sim 4\,\text{THz}$.

We model the THz photoconductivity of the samples, σ_L, as a sum of Lorentzian oscillators, typical of resonances in excitonic systems. Here,

$$\Delta\sigma_\text{L} = \sum_m \frac{C_m i \nu}{\nu^2 - \nu_{0m}^2 + i\nu\gamma_m}, \tag{1}$$

where C_m is a spectral weight coefficient, ν_0 is the resonant frequency and γ_m is the linewidth of oscillator m.

Free charges, as opposed to excitonic resonances, are characterised by the Drude conductivity, which is just the special case of a Lorentzian spectrum with $\nu_{0_\text{Drude}} = 0$, giving a functional form with a peak in $\text{Re}(\sigma)$ at $\nu = 0$ (the DC Drude conductivity). In contrast excitons, which are polarisable and exhibit no DC conductivity have a resonant frequency ν_{0_X} characteristic of their dominant (usually $1s \rightarrow 2p$) transition.[5]

As discussed in the main paper, trions have recently been observed in monolayer MoS_2. These quasiparticles consist of two electrons bound with a hole, and should also show a Lorentzian type photoconductivity spectrum, with an oscillation frequency equal to the additional binding energy of the trion over a normal exciton.

Due to the small signal from these samples, it is very difficult to find an accurate fit to the data. However, we present the parameters of a potential fit in Supplementary Table 2, comparing the contributions from Drude photoconductivity (σ_D), excitons (σ_X) and trions (σ_T), found from a least squares fitting algorithm weighted to account for the THz spectral intensity of the system.

As the high frequency oscillation in trilayer MoS_2 and monolayer WSe_2 is far out of the bandwidth of the THz spectrometer, the oscillation frequency cannot be found from fitting. A value of $25\,\text{THz}$ ($100\,\text{meV}$) was therefore chosen as a reasonable approximation for the exciton binding energy[6–8]. Additionally, the literature value of trion binding energy in monolayer MoS_2, $18\,\text{meV}$,[22] was fixed for the monolayer MoS_2 fit.

Table S2: THz photoconductivity fitting parameters.

		MoS$_2$ Mono	WSe$_2$ Mono	MoS$_2$ Tri†
σ_D	C$_{\text{Drude}}$(%)	7.4 ± 2.6	2 ± 1.4	2
	γ (THz)	1.35 ± 0.34	4.76 ± 2.8	9
σ_X	C$_X$(%)	–	97.6 ± 1.6	76
	γ (THz)	–	8 ± 30	5
	ν_{0_X} (THz)	–	25*	25*
σ_T	C$_T$(%)	92.6 ± 2.6	0.4 ± 0.2	22
	γ (THz)	10.1 ± 1.4	0.84 ± 0.32	14
	ν_{0_T} (THz)	4.4*	3.3 ± 0.07	4.4*

*Value held fixed in fitting routine
† Errors not given due to large uncertainty in values far outside of the experimental bandwidth

Figure S5 shows a comparison of least square fits to monolayer WSe$_2$ photoconductivity spectra with (green solid line) and without (red broken line) a high frequency, 25 THz oscillator. The measured data are shown as blue crosses. The best fit is achieved when a 3.3 THz oscillator and a 25 THz oscillator are included. The parameters for the fit without the high frequency oscillator are: C$_{\text{Drude}} = 8\%$, $\gamma_{\text{Drude}} = 1.95$ THz, C$_T = 92\%$ $\gamma_T = 5.63$ THz, $\nu_{0_T} = 6.98$ THz.
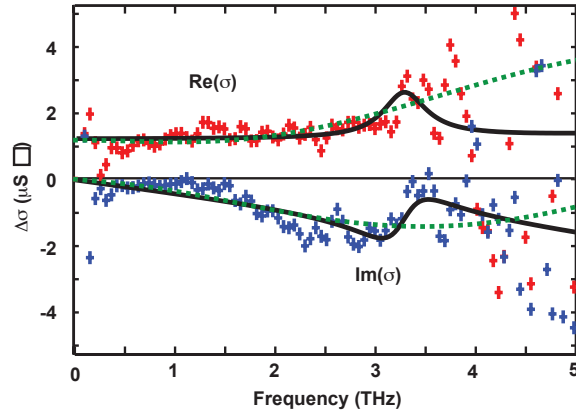

Figure S5: Measured AC photoconductivity spectrum of Monolayer WSe$_s$ (blue points), fitted by two possible models using a least squares fitting routine. The solid black line shows a 3-oscillator fit where the two high frequency oscillators correspond to an exciton resonance and a trion resonance. The green dashed line shows a two-oscillator fit, excluding the trion resonance.

Spectra of Laser Pump Beams

In Supplementary Figure S6, the spectra of the pump beams used in the experiments is shown. Two different excitation energy ranges were used during the measurements. For experimental reasons, slightly different pump energies were used for the THz and PL measurements. For low energy excitation, on resonance with the excitons at the K point, the samples were photoexcited with 1.9 eV photons (650 nm) for THz measurements, and 2.1 eV photons (600 nm) for PL measurements. For above gap excitation, 3.1 eV photons (400 nm) and 3 eV (410 nm) were used for THz and PL respectively. The behaviour of the samples within these energy ranges was observed to be the same.
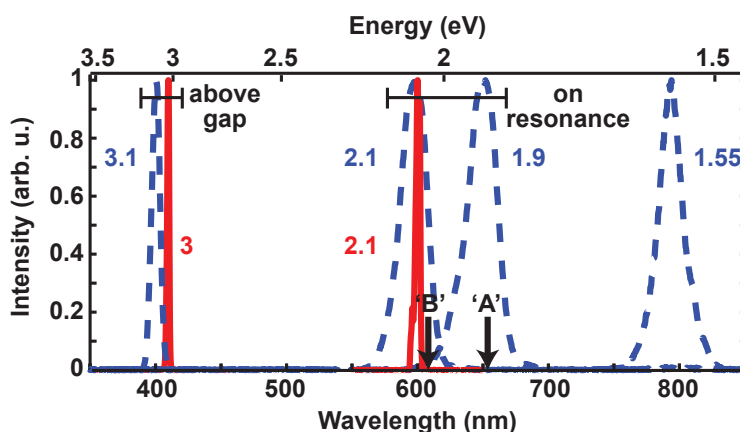

Figure S6: Spectra of the pump beams used for THz (blue dotted lines) and PL (red solid lines) measurements. 1.9 eV (650 nm) and 2.1 eV (600 nm) photons were used to photoexcite the samples on resonance with the excitons. Above gap energies of 3.1 eV (400 nm) for THz and 3 eV (410 nm) for PL were used for higher energy photoexcitation. Arrows demonstrate the position of the 'A' and 'B' excitons.

Pump Energy Dependence of THz Photodynamics

Monolayer MoS_2 was photoexcited at varying pump energies, and the subsequent dynamics measured by optical pump–THz probe spectroscopy. As can be seen in Supplementary Figure S7, the dynamics are nearly identical when the sample was photoexcited with 2.1 eV (600 nm) photons or 1.9 eV (650 nm), justifying the comparison of 1.9 eV THz data with 2.1 eV pumped PL mea-

surements in Figure 4 of the main paper. Furthermore, when photoexcited with 1.55 eV (800 nm) photons, i.e. below the band gap, no photoinduced response is observed.
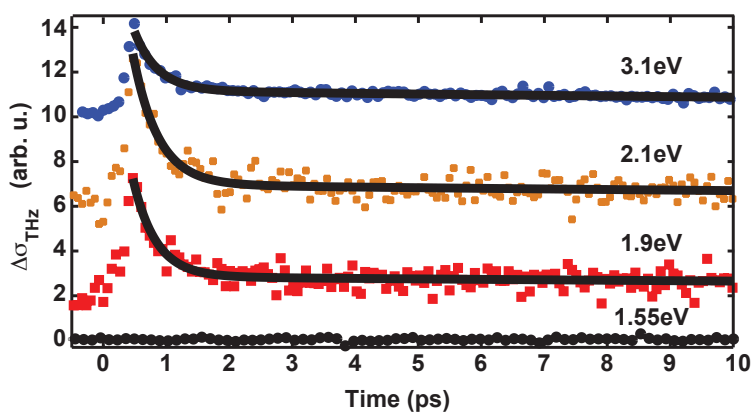

Figure S7: Photoinduced THz conductivity, $\Delta\sigma_{THz}$, of monolayer MoS_2 as a function of time after photoexcitation. Excited with pump beam energies of, from top to bottom, 3.1 eV (400 nm), 2.1 eV (600 nm), 1.9 eV (650 nm) and 1.55 eV (800 nm). The photoexcited dynamics are identical for 2.1 eV and 1.9 eV photoexcitation. The solid lines represent biexponential fits to the data.

Pump Fluence Dependence of THz Photoconductivity

The magnitude of the pump induced change in THz transmission intensity (proportional to the square of the induced THz photoconductivity) was also measured as a function of pump fluence. As can be seen in Supplementary Figure S8 for photoexcitation with 3 eV photons, the induced transmission intensity varies linearly with pump fluence in the regime used in these experiments.

Removal of Reflections from Trilayer Data

Due to the thinness of the sapphire substrate, the optical pulse used in optical pump–THz probe measurements was able to reflect from the far edge of the substrate and re-photoexcite the sample before the signal from the initial excitation had decayed. This manifested itself as additional peaks within the pump–probe data, as can be seen in Supplementary Figure S9. For clarity, these peaks were removed from the data presented in the main paper by adopting a biexponential decay model
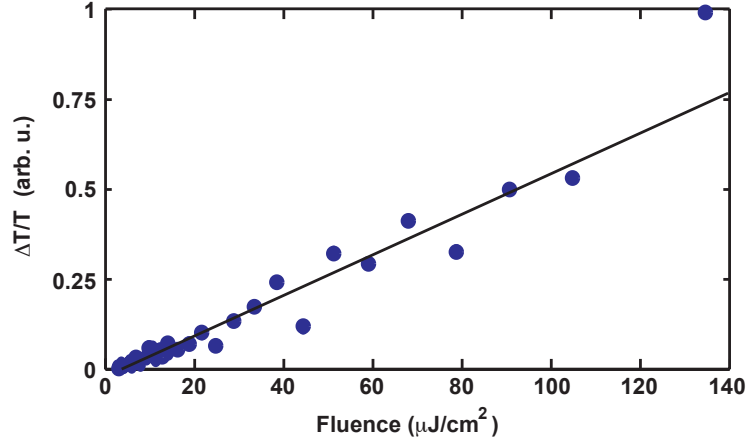
Figure S8: Fluence dependence of the peak pump induced THz transmission intensity change, $\Delta T/T$. Measured on monolayer MoS_2 using $3\,eV$ ($400\,nm$) photons. The solid black line is a least squares fit to the data, showing the linear relationship between fluence and transmission intensity change.
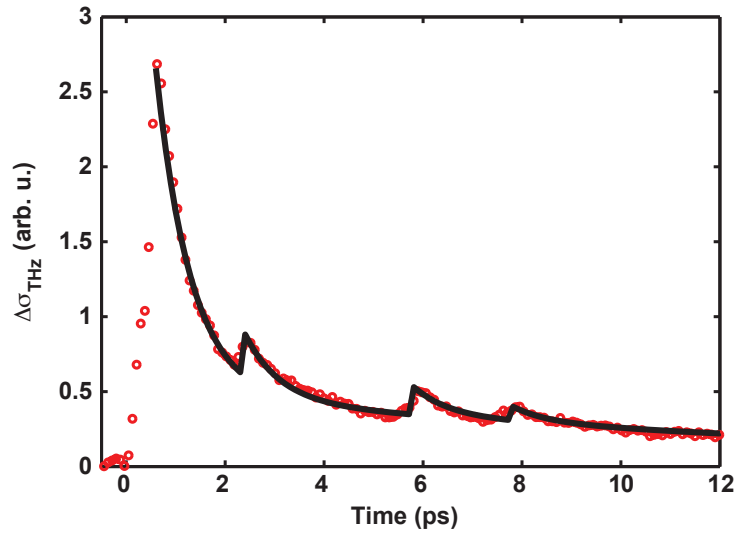

Figure S9: Original trilayer optical pump–THz probe data, shown here for $1.9\,eV$ ($650\,nm$) photoexcitation, before removal of reflections from the data. Red dots show the measured data, the solid line is a biexponential model to the data accounting for multiple substrate reflections.

with additional terms for subsequent smaller excitations, and then subtracting the subsequent excitation terms from the data. This effect of reflections within the substrate was only observable in the trilayer data, as it is too small an effect to be visible in the smaller $\Delta E_{THz}/E_{THz}$ of the monolayer sample.

References

1. Pu, J.; Yomogida, Y.; Liu, K. K.; Li, L. J.; Iwasa, Y.; Takenobu, T. Highly Flexible MoS_2 Thin-film Transistors with Ion Gel Dielectrics. *Nano Lett.* **2012**, *12*, 4013–4017.

2. Huang, J. K.; Pu, J.; Hsu, C. L.; Chiu, M. H.; Juang, Z. Y.; Chang, Y. H.; Chang, W. H.; Iwasa, Y.; Takenobu, T.; Li, L. J. Large-area Synthesis of Highly Crystalline WSe_2 Mono Layers and Device Applications. *ACS Nano* **2014**, *8*, 923–930.

3. Ulbricht, R.; Hendry, E.; Shan, J.; Heinz, T. F.; Bonn, M. Carrier Dynamics in Semiconductors Studied with Time-resolved Terahertz Spectroscopy. *Rev. Mod. Phys.* **2011**, *83*, 543–586.

4. Lloyd-Hughes, J.; Jeon, T.-I. A Review of the Terahertz Conductivity of Bulk and Nano-materials. *J Infrared Milli Terahz Waves* **2012**, *33*, 871.

5. Kaindl, R. A.; Hägele, D.; Carnahan, M. A.; Chemla, D. S. Transient Terahertz Spectroscopy of Excitons and Unbound Carriers in Quasi-two-dimensional Electron-hole Gases. *Phys. Rev. B* **2009**, *79*, 045320.

6. Goto, T.; Kato, Y.; Uchida, K.; Miura, N. Exciton Absorption Spectra of MoS_2 Crystals in High Magnetic Fields up to 150T. *J. Phys.-Condes. Matter* **2000**, *12*, 6719–6723.

7. Coehoorn, R.; Haas, C.; Degroot, R. A. Electronic-structure of $MoSe_2$, MoS_2, and WSe_2. II The Nature of the Optical Band-gaps. *Phys. Rev. B* **1987**, *35*, 6203–6206.

8. Komsa, H. P.; Krasheninnikov, A. V. Effects of Confinement and Environment on the Electronic Structure and Exciton Binding Energy of MoS_2 from First Principles. *Phys. Rev. B* **2012**, *86*, 241201.